Journal of Atmospheric and Solar-Terrestrial Physics 188 (2019) 26–43

Contents lists available at ScienceDirect

Journal of Atmospheric and Solar-Terrestrial Physics

journal homepage: www.elsevier.com/locate/jastp

Aerosol and gaseous pollutant characteristics during the heating season (winter–spring transition) in the Harbin-Changchun megalopolis, northeastern China

Hujia Zhao[a,b], Yanjun Ma[a,*], Yaqiang Wang[b], Hong Wang[b], Zhizhong Sheng[c,b], Ke Gui[b], Yu Zheng[b], Xiaoye Zhang[b], Huizheng Che[b]

[a] Institute of Atmospheric Environment, China Meteorological Administration, Shenyang, 110016, China
[b] State Key Laboratory of Severe Weather (LASW) and Key Laboratory for Atmospheric Chemistry, Institute of Atmospheric Composition, Chinese Academy of Meteorological Sciences, CMA, Beijing, 100081, China
[c] Plateau Atmospheric and Environment Laboratory of Sichuan Province, College of Atmospheric Science, Chengdu University of Information Technology, Chengdu, 610225, China

ARTICLE INFO

Keywords:
Aerosol pollutants
Lidar
Residential heating
Northeastern China

ABSTRACT

Serious pollution events caused by residential heating activities occur frequently in northeastern China, and these increased particulate matter levels and gaseous pollutants could contribute to both local emissions and regional climate change. In this study, meteorological data, air trajectories and aerosol vertical distributions were used to study the pollutant sources and movement paths during the heating season (winter–spring transition) in the Harbin-Changchun megalopolis, northeastern China. Higher concentration of fine-mode particles ($PM_{2.5}/PM_{10}$ ~ 0.70–0.80) and the trace gas SO_2 (35–45 μg m^{-3}) could be seem as an indicator of the air quality in the Harbin-Changchun megalopolis during the residential heating seasons, caused by local emissions. The apparent changes of meteorological elements in the high latitude and cold regions over Northeastern China could have important effects on the pollutant formation, secondary transformation, aerosol accumulation and vertical transport over the heating season. The $PM_{2.5}$ concentrations were highly associated with the SO_2 and NO_2 from both fossil fuel combustion and biomass burning. The obvious diurnal pollutants variation shown thermodynamic conditions could be considered one of the important environmental elements responsible for residential heating processes. The mixture effect of local emissions and aerosol convective activities were found to contribute to the aerosol extinction and air pollution in the Harbin-Changchun megalopolis. These findings could help to improve our understanding of the association between aerosol pollutants influenced by the anthropogenic activities and the aerosol regional climate effects during the heating season in northeastern China.

1. Introduction

Aerosols in the atmosphere change the energy balance between the earth and atmospheric systems (Okada et al., 2001; Watson, 2002; Megido et al., 2017; Shantikumar et al., 2014, 2015). As anthropogenic activities increase, fine particulate matter (PM) has been increasingly studied as the key air pollutant originating from natural and anthropogenic sources and is composed of primary and secondary particles (Pathak et al., 2009; Tiwari et al., 2009). In particular, the high level of $PM_{2.5}$ derived from industrial activities, fossil fuel combustion and biomass burning has been studied in many reports (Andreae et al., 2006; Bahadur et al., 2009; Kirpa and Sarin, 2011; Tzompa et al., 2016).

It is worth noting that the sharp increase of air pollutants (e.g., PM_{10}, $PM_{2.5}$, SO_2, NO_2, CO and O_3) concentrations in the short term, especially those resulting from the coal combustion during heating season in China, has become one of the most important drivers of severe winter pollution (Wang et al., 2003; Shen et al., 2013; Q. Li et al., 2017a, b; Chen et al., 2017). The National Bureau of Statistics of China (NBSC, 2016) reported that China accounts for about half of the global annual coal consumption, and large amounts of PM and gaseous pollutants are generated, which are associated with the residential heating during winter (Bond et al., 2004; Cao et al., 2006; Zhang et al., 2008, 2017a, 2017b). Many studies have shown a major contribution from residential coal burning emissions to the winter haze formation in China (Liu et al., 2016; Chen et al., 2017; Li et al., 2018; Zhang et al.,

* Corresponding author. 388 Changbai South Road, Shenyang, 110016, China.
E-mail address: tjzhj4659@sina.com (Y. Ma).

https://doi.org/10.1016/j.jastp.2019.03.001
Received 23 January 2019; Received in revised form 23 February 2019; Accepted 1 March 2019
Available online 27 March 2019
1364-6826/ © 2019 Published by Elsevier Ltd.

2018b).

Geographically, northeastern China is located at high latitude, with a longer and harsher winter compared with other regions of China. Therefore, the heating season in northeastern China begins earlier in October and lasts longer through April in the following year. As a result of the unique pattern of anthropogenic emissions of the residential heating activities during winter in northeastern China, the changes of PM levels contributing to the local emissions could lead to regional climate change (Zhao et al., 2015, 2018a, 2018b; Shen et al., 2011; Zhang et al., 2012; Kong et al., 2012; Qiao et al., 2010; Huang et al., 2014). The Harbin-Changchun megalopolis is an important equipment manufacturing and grain production base located in the hinterland of northeast China including two core cities of Harbin and Changchun. These typical winter central heating cities are typically affected by residential heating throughout winter until spring in the following year.

This work focuses on the variations of air pollutants (including $PM_{2.5}$, PM_{10}, SO_2, CO, NO_2 and O_3) at the Harbin-Changchun megalopolis, northeastern China, during the heating season in 2017/2018. The visibility, meteorological data (including wind speed, temperature and relative humidity (RH)), and aerosol vertical information based on the lidar, were used to illustrate the characteristics of PM and gaseous pollutants during the pollution process. Moreover, the backward trajectory and weight potential source contribution function (WPSCF) was used to obtain $PM_{2.5}$ potential sources and transmission paths during the sampling period. The findings of this study could also have important reference value in energy control and emission reduction in northeast China, especially in the air quality improvement during the residential coal burning period.

This paper is divided into the following parts: Section 2 introduces the observation sites and data used to describe the characteristics of pollutants during heating from the transition season. Section 3 examines the periodic variation of pollutants concentration and meteorological elements, as well as the corresponding relationship during the different heating stages. Section 3 also includes a case analysis in which the aerosol vertical properties based on the ground-based lidar and the pollutant potential sources by the backward trajectory model are discussed. Finally, conclusions are given in Section 4.

2. Materials and methods

2.1. Sample collection

The geographical location of the three sampling sites (Harbin, Changchun and Siping) in northeastern China is shown in Fig. 1.

Harbin (45.75°N, 126.77°E, 143 m, asl) is the capital of Heilongjiang province with a population of 9,952,000. Harbin is the northernmost city in northeast China and experiences a severe cold winter. Changchun (43.88°N, 125.35°E, 138 m asl) is another central city in northeastern China. It is the capital of Jilin province with a population about 7,672,000. It is an important industrial base and comprehensive transportation hub and represents an important node city of the "One Belt And One Road" northern line, and a core city of the Harbin-Changchun megalopolis. Siping (43.17°N, 124.37°E, 138 m asl) is a prefecture-level city in Jilin province, with a smaller population about 3,204,000. This city is the only route from Jilin, Heilongjiang and eastern Inner Mongolia to the Yangtze River Delta and the Beijing-Tianjin-Hebei region. Yushu (44.83°N, 126.55°E, 143 m, asl), a county-level city about 160 km from Changchun, is located at the centre of a triangle of Changchun, Jilin and Harbin.

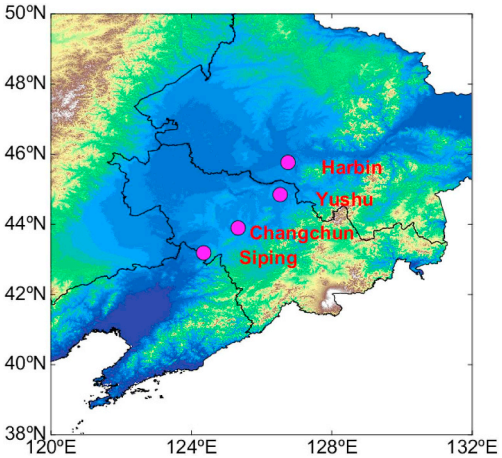

Fig. 1. Locations of the sampling sites in the Harbin-Changchun megalopolis, northeastern China.

In terms of climatic characteristics, residents of the three cities endure a long and cold winter, and coal combustion is widely used for household heating (Chen et al., 2018). Therefore, the selection of the above areas can be considered representative for research on regional pollution events, which are strongly associated with coal heating emissions during the whole study period in northeastern China. In this study, the sampling periods were divided into three stages: the heating season from 1 December to 31 March, the transition period from 1 to 30 April, and the non-heating season from 1 to 31 May.

2.2. Measurement and data

A ground-based Micro Pulse Lidar-DSL-A031-F (Darsunlaser Co., Ltd, Shenzhen, China) has been installed at two observation sites at Harbin and Yushu since November 2017. The instrument has been standardized and calibrated to ensure high data quality during the residential heating campaign. This lidar provides backscattering at 1064 nm based on Mie scattering theory, with a temporal resolution of approximately 1 min and a vertical resolution of approximately 15 m. The aerosol vertical profiles including aerosol extinction coefficients and PBL were also derived from the lidar products.

The PM (including PM_{10} and $PM_{2.5}$) and gaseous pollutants (including SO_2, CO, NO_2 and O_3) mass concentration data were obtained from the China air quality online monitoring and analysis platform (https://www.aqistudy.cn/) from 1 December 2017 to 31 May 2018.

The meteorological data of wind speed, temperature and RH were also obtained at the observation station from 1 December 2017 to 31 May 2018.

The wind fields at 1000 and 850 hPa, from the European Centre for Medium-Range Weather Forecasts ERA-Interim dataset (https://www.ecmwf.int/) were obtained to analyze the regional weather field during sampling times.

2.3. Statistical methods

The 72-h backward trajectories with 2 h interval each day were calculated and bunched into clusters using the TrajStat software (http://www.meteothink.org/products/trajstat.html) with a starting height of 200 m above ground level (Wang et al., 2006). Two models with a weight function applied were used to illustrate the spatial distributions of potential $PM_{2.5}$ sources on the prevailing transport trajectories: the WPSCF and the concentration-weighted trajectory (WCWT).

The Potential Source Contribution Function (PSCF) analysis was used to calculate the probability of a source located at latitude i and longitude j. The PSCF value of the grid cells are calculated by counting the trajectory segment endpoints based on the TrajStat results to terminate in each cell by the following equation:

$$PSCF_{ij} = m_{ij} / n_{ij} \quad (1)$$

where n_{ij}: the whole number of the end points fall in the cell (i,j); m_{ij}: the number of a source concentration higher than the threshold

criterion value when the trajectories passed through the cell (*i,j*). In this study, the criterion value was set to 75 μg m −3 of a source of $PM_{2.5}$ according to China's national ambient air quality standard (GB3095-2012: http://kjs.mep.gov.cn/hjbhbz/bzwb/dqhjbh/dqhjzlbz/201203/t20120302_224165.htm).

A weight function W_{ij} was multiplied to the PSCF value in order to reduce the effect of smaller n_{ij} reported in Wang et al. (2009):

$$\mathrm{WPSCF} = W_{ij} \times \mathrm{PSCF} \tag{2}$$

$$W_{ij} = \begin{cases} 1.0, & 3n_{ave} < n_{ij} \\ 0.7, & 1.5n_{ave} < nij \le 1.5n_{ave} \\ 0.2, & n_{ij} \le n_{ave} \end{cases} \tag{3}$$

where n_{ave} the average trajectory points in all grid cells contain at least one trajectory point; n_{ij} the number of the included trajectory points in the cell (*i,j*).

The Concentration Weighted Trajectory (CWT) analysis was implemented in this paper to localize major sources of $PM_{2.5}$ emission. As Equation (4) shown, the values were multiplied with a same weight function (W_{ij}) as PSCF was used in order to minimize the uncertainty of CWT value.

$$C_{ij} = \frac{\sum_{k=1}^{M} C_k \times \tau_{ijk}}{\sum_{i}^{M} \tau_{ijk}} \times W(i,j) \tag{4}$$

Where c_{ij}: the weighted average concentration in a grid cell (*i,j*); C_k: the measured concentration at the sampling site during the residence time;: the residence time of the backward trajectories corresponding to in grid cell (*i,j*). The PSCF and CWT analysis in this study was analyzed on a 0.5° × 0.5° resolution grid.

3. Results and discussion

3.1. Temporal variation in PM and gaseous pollutants during the whole heating season

High concentrations of the fine-mode particles were found in all three sites within the Harbin-Changchun megalopolis during the sampling period (Fig. 2). During this time, observation days with $PM_{2.5} > 75\ \mu g\ m^{-3}$ lasted for 48, 25 and 38 days and accounted for 26.4%, 13.7% and 20.9% of the total observation days in Harbin, Changchun and Siping, respectively. However, these pollutant days ($PM_{2.5} > 75\ \mu g\ m^{-3}$) were concentrated in the heating season, accounting for 35.5%, 19.8% and 30.0% of the total observation days in the sampling days over the three sites, respectively. The concentration of coarse-mode particles showed a clear surge in the heating season (Fig. 2). The maximum PM_{10} mass concentration reached 398.9 μg m^{-3} on 17 April 2018 in Harbin. This result could be due to the spring dust in northeastern China (Zhang et al., 2018b). The ratio of $PM_{2.5}/PM_{10}$ increased to about 0.70–0.80 show a transition of fine-mode particle fraction in the heating season, which was larger than at the end of the period with lower ratio decreased to 0.40–0.50.

The variation of gas pollutants in the three major cities in the Harbin-Changchun megalopolis is also described in Fig. 2 during the study period. It is interesting to note that the SO_2 concentration remained high during the heating season. The average values of SO_2 during the heating season ranged from 35 to 45 μg m^{-3} across the three regions. From the transition to the non-heating season, the SO_2 concentration sharply decreased to about 6.0–8.0 μg m^{-3}, with completely ceased heating activities. These results indicate that the residential heating contributes the majority of SO_2 in northeastern China. As reported by Zhang et al. (2009) for northern China, fossil fuel use during the heating season could also contribute to the emission of trace gases such as CO and NO_x. However, in this paper, the variation trend of NO_2 and CO was not as major as that of SO_2. The CO mainly showed a trend of slow decline, with an average value range from 0.5 to 1.2 mg m^{-3} from the heating to non-heating sampling period for the three sites. In addition, NO_2 had a tendency to fluctuate with an average value range from 20.0 to 40.0 μg m^{-3} in the whole heating period at the three sites. There was no obvious downward trend of NO_2 concentration in the later heating season, which could be because of the increasing biomass-burning emissions as heating demand gradually declined in March and April. The change of O_3 was quite different to the other gas pollutants. The lower concentration of O_3 has firstly been found in the heating time about 50 μg m^{-3} in the three sites under lower temperature. At the end of the heating season, the longer and stronger solar irradiation could favor photochemical formation of O_3. The O_3 concentration increased to 80–100 μg m^{-3} at all sites.

Therefore, the variation of PM and gas pollutants during the coal combustion period indicates that fine-mode particles and trace gases such as SO_2 could be caused by local emissions from heating sources, which may act as an indicator of the air quality in the Harbin-Changchun megalopolis. In contrast, the large number of coarse-mode aerosols and NO_2 were more likely attributed to spring dust and the fractional contribution of biomass burning from the transition to the non-heating season (Li et al., 2019).

3.2. Monthly variation in meteorological elements during the whole heating season

Table 1 shows the temporal variation of wind speed, temperature and RH during the study period to facilitate understanding of the effects of ground-surface meteorological conditions on air quality.

Slightly weaker winds with an average value of about 1.0–2.0 m s^{-1} were found in Harbin, Changchun and Siping in December and January, which could limit the dispersion of pollutants in the cold season. The lowest windspeeds of < 1.0 m s^{-1} mainly occurred in February during the serious pollution period of the heating season. The significantly lower wind speeds about 0.5–0.7 m s^{-1} could cause a high PM accumulation. At the end of the heating season, the increasing wind speed with an average value of about 3.0–4.0 m s^{-1} in March to May could decrease the aerosol concentration. At the same time, we also found a considerably larger wind speed in Siping with an average value about 4.5 m s^{-1} in April in the transition period than in other cities.

The strong wind in the later period of heating may help to carry a considerable aerosols from the surrounding area to Siping by regional transportation, which could be another important factor causing air quality deterioration. Li et al. (2015) indicated that pollution may be transported from Harbin to Changchun during haze and fog pollution episodes over northeastern China.

In terms of temperature, the lower temperatures occurred in Harbin with an average value of nearly −19.5 °C in January during the heating season. This was nearly 5 °C higher than that at Changchun (−15.6 °C) and Siping (−16.8 °C) at the same time. Changchun and Siping are positioned at a lower latitude than Harbin and thus the beginning time of heating season in Harbin is earlier than Changchun and Siping. Therefore, the accumulation of emission sources will have an impact on air quality to some extent. As the season changed, the heating activities decreased and a higher temperature (about 9.0–11.0 °C) was correspondingly found in the Harbin-Changchun megalopolis in April. Due to the change of solar elevation angle and the further increased radiation, the temperature reached 16.0–18.0 °C by the end of the heating season in May.

Apparent temperature changes have important effects on secondary formation of aerosol and the chemical transformation of gaseous pollutants. The solar radiation and air temperature have unique contributions to the O_3 concentration through photochemical reactions and the indirect impact on the levels of the corresponding precursors such as CO and NOx (Zhang et al., 2018a).

The variation of RH showed a peak value in December and January during the heating season with an average about 60.0%–66.0% in Harbin, Changchun and Siping. In contrast, in the late heating season,

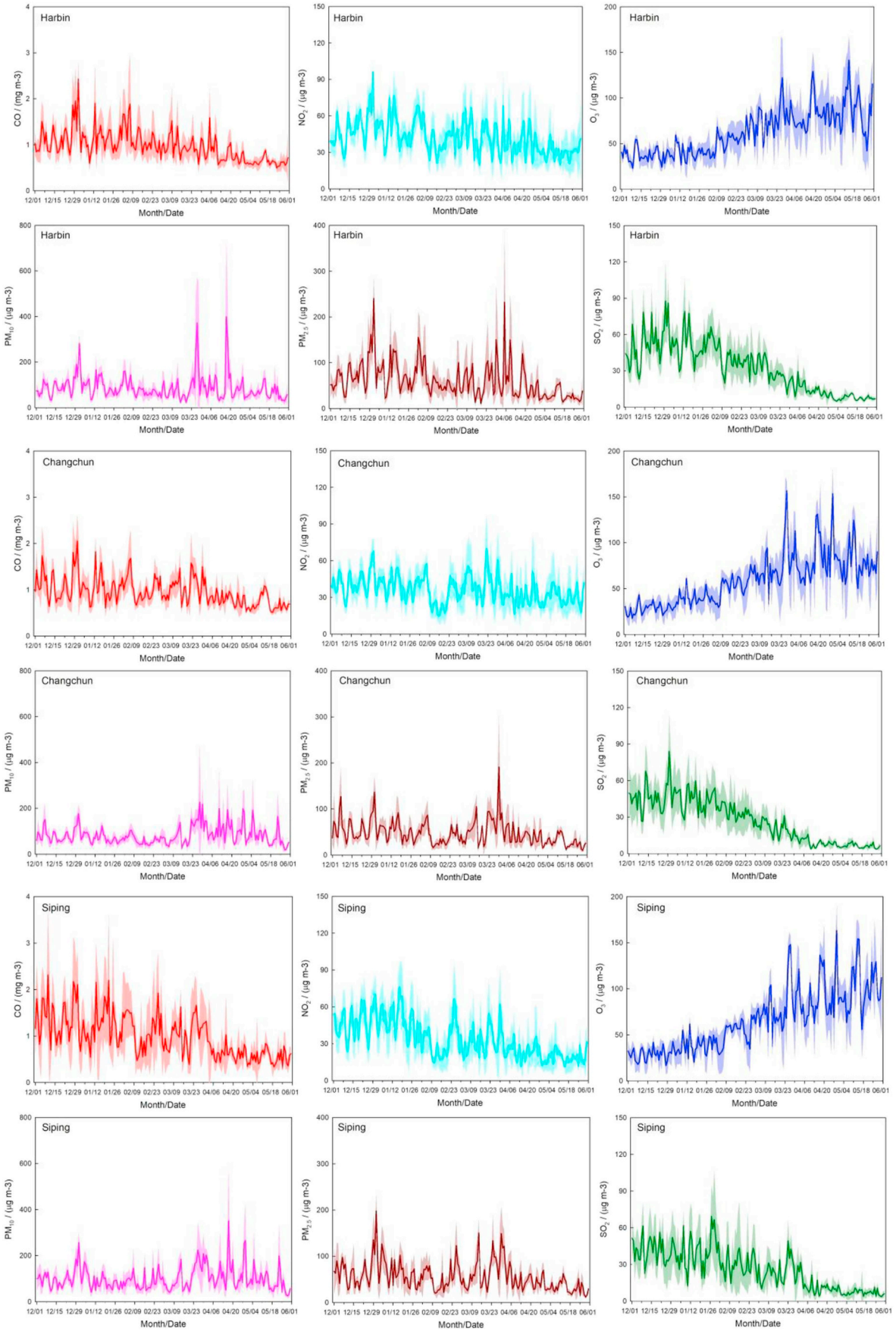

Fig. 2. Temporal variation in PM and gas pollutants during the whole heating season at the three sites in the Harbin-Changchun megalopolis, northeastern China. The shaded area represents the standard deviations of the arithmetic means.

Table 1
Monthly variation of meteorological elements during the whole heating season at Harbin, Changchun and Siping. Data presented here are shown as arithmetic mean ± standard deviation.

Site		December	January	February	March	April	May
Harbin	Wind speed/(m s^{-1})	1.9 ± 1.2	2.0 ± 1.1	0.9 ± 1.3	3.0 ± 2.1	3.3 ± 2.1	2.8 ± 1.8
	Temperature/(°C)	−17.0 ± 5.1	−19.5 ± 6.5	−16.3 ± 5.8	−3.6 ± 10.4	9.0 ± 7.2	16.3 ± 5.6
	RH/(%)	66.1 ± 12.5	66.2 ± 11.9	63.3 ± 13.5	57.1 ± 20.2	46.5 ± 24.4	49.7 ± 22.2
Changchun	Wind speed/(m s^{-1})	1.8 ± 1.3	2.0 ± 1.2	0.7 ± 1.1	2.7 ± 1.9	3.3 ± 1.9	2.5 ± 1.7
	Temperature/(°C)	−12.3 ± 5.2	−15.6 ± 6.5	−12.3 ± 5.5	−0.5 ± 9.5	10.6 ± 7.4	16.8 ± 5.2
	RH/(%)	59.8 ± 13.2	59.9 ± 13.3	52.3 ± 16.1	53.4 ± 21.5	37.1 ± 21.7	47.9 ± 23.4
Siping	Wind speed/(m s^{-1})	2.0 ± 1.8	1.7 ± 1.6	0.7 ± 1.1	3.4 ± 2.8	4.5 ± 3.2	3.4 ± 2.4
	Temperature/(°C)	−12.0 ± 6.0	−16.8 ± 7.8	−12.6 ± 6.6	−0.1 ± 9.5	10.6 ± 7.5	17.4 ± 5.5
	RH/(%)	61.4 ± 15.5	64.3 ± 17.1	52.6 ± 18.2	57.2 ± 25.0	40.6 ± 24.3	46.6 ± 24.1

the RH value fell to a lower average value of about 53.0%–57.0%. In April and May, the RH further decreased to < 50.0% by the transition of heating season. With the higher temperature, the larger RH could be more favorable to the higher concentration of fine-mode particles through the secondary aerosol photochemical transformation (Hennigan et al., 2008).

3.3. Periodic variation in air pollutants and meteorological elements during the different heating stages

In this section, we analyze the variation of PM ($PM_{2.5}$ and PM_{10}) and gas pollutant concentrations (SO_2, NO_2, CO and O_3) as well as RH, wind speed and temperature during the heating, transition and non-heating season. These analyses were conducted to improve our understanding of the effects of heating emissions on the regional air quality.

The PM_{10} concentration in the heating season was a little lower in Harbin, Changchun and Siping (90.2, 77.7 and 96.5 μg m^{-3}, respectively) than that in the transition time (98.8, 106.1 and 126.6 μg m^{-3}, respectively) (Fig. 3a). At the end of the heating season, the PM_{10} concentration was deceased to an average value of 63.4, 74.1 and 85.1 μg m^{-3} in Harbin, Changchun and Siping, respectively. This indicates that the coarse-mode particles were not a major pollutant during heating season in the Harbin-Changchun megalopolis.

Unlike PM_{10}, the concentration of $PM_{2.5}$ was highest in the heating season s with a maximum average value about 69.4, 53.1 and 64.0 μg m^{-3} in Harbin, Changchun and Siping, respectively. The higher $PM_{2.5}$ concentrations in heating season indicate high emissions from coal burning for domestic heating in northeastern China. As the heating activities weakened in the transition period, the $PM_{2.5}$ mass concentration decreased to about 59.8, 43.4 and 50.2 μg m^{-3} in Harbin, Changchun and Siping, respectively. The minimum $PM_{2.5}$ concentrations occurred during the non-heating season, with an average value of about 27.9, 28.0 and 31.5 μg m^{-3} in Harbin, Changchun and Siping, respectively, which was almost 2.0 times lower than that in the heating season at the three sites.

The variations of gaseous pollutants including SO_2, NO_2, CO and O_3 during the different heating stages were also observed. The SO_2 concentrations were high during the heating season s at the three sites (43.6, 36.7 and 34.3 μg m^{-3}), moderate in the transition period (14.6, 9.1 and 11.5 μg m^{-3}) and began to decline sharply in the non-heating (7.5, 6.2 and 6.7 μg m^{-3}) period in Harbin, Changchun and Siping, respectively. The maximum SO_2 concentrations during the heating season were almost 5.0–6.0 times higher than those in the non-heating season at the three sites. These results suggest that the dominant source of SO_2 is coal burning in northeastern China. The higher NO_2 concentrations in the heating season were about 46.6, 39.2 and 40.7 μg m^{-3} in Harbin, Changchun and Siping, respectively. It is worth noting that the NO_2 concentrations did not decline as dramatically as those of SO_2, but were similar during the transition (38.2, 31.4 and 23.5 μg m^{-3}) and non-heating season s (30.9, 30.7 and 19.2 μg m^{-3}) in Harbin, Changchun and Siping, respectively. This could be because of the increased open fires (biomass) from the transition period to the non-heating season (Fig. 2), because biomass burning was also one of the important sources of NO_2 during the non-heating season. The highest CO concentrations at the three sites were about 1.1–1.2 mg m^{-3} in the heating season, whereas lower CO concentrations were recorded in the transition and non-heating season, with values of 0.7–0.8 and 0.5–0.7 mg m^{-3}, respectively. As the season changed from the heating season to the non-heating season, there were fewer sources of CO in the region. The variations of O_3 concentration were opposite to those of the pollutants listed above during the whole period (Fig. 2). The lowest O_3 concentrations were observed in the heating season with values of 50.9, 47.3 and 49.0 μg m^{-3} in Harbin, Changchun and Siping, respectively, which increased to 84.5, 78.1 and 99.8 μg m^{-3}, respectively, during the non-heating season. The higher O_3 concentrations during the non-heating season were almost 1.7–2.0 times higher than those in the heating season at the three sites. Solar radiation is likely to be the main factor in O_3 formation, which contrasts with other gas pollutants at higher temperatures. Lower levels of O_3 could be attributed to the weak solar radiation during the heating season under lower temperatures.

Fig. 3b shows the meteorological elements during the different stages of the whole heating season. The significant change of temperature in the whole period shows that the temperature was substantially lower in heating season below zero about −14.0, −10.1 and −10.2 °C in Harbin, Changchun and Siping, respectively. At the end of heating season, the temperature increased to 16.4, 16.9 and 17.5 °C. The change of ambient temperature is conducive to the pollutant conversion through the gas–particle transformation and photochemical reactions. Wind speed is a parameter that could indicate pollution dilution effects on air quality. The weaker windspeed (1.8–1.9 m s^{-1}) in the heating season was not conducive to pollutant diffusion, whereas the stronger wind in the transition and non-heating in Harbin, Changchun and Siping (2.8–3.4, 2.6–3.3 and 3.4–4.5 m s^{-1}) could cause regional pollution transportation. The variation in RH was another major meteorological factor during the heating season. The average RH was about 63.2%, 56.4% and 59.0% in Harbin, Changchun and Siping, respectively, which was more conducive to the pollution occurring during the heating season. At the end of the heating season, the RH decreased to 40.0%–50.0%.

3.4. Relationship between PM and gaseous pollutants during the different heating stages

The correlations between $PM_{2.5}$ and temperature and RH, as well as the relationships among SO_2, NO_2, O_3 and CO are illustrated in Fig. 4 during the heating, transition and non-heating season s at the three sites.

Taking Harbin as an example, the correlation between $PM_{2.5}$ and air temperature was divided into different parts. The lowest temperature was below zero during most of the heating season. The $PM_{2.5}$ mass concentrations almost reached 300 μg m^{-3}, which was mainly caused by the pollutant discharge in the heating season. As the heating

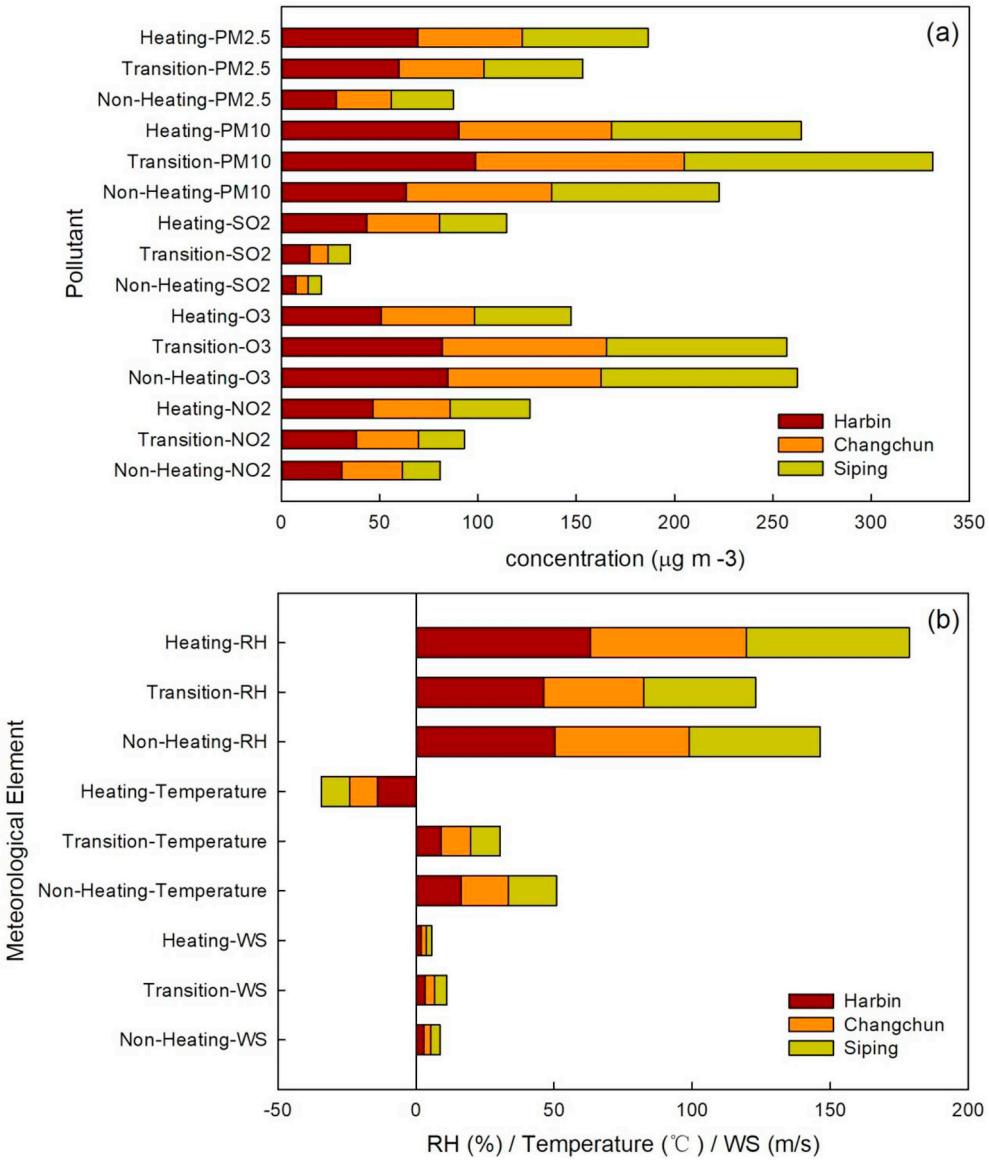

Fig. 3. Periodic variation in (a) air pollutants and (b) meteorological data during the different heating stages at Harbin, Changchun and Siping. The heating period range from 1 December to 31 March, the transition period range from 1 to 30 April, and the non-heating period range from 1 to 31 May.

activities began to decrease, the temperature ranged from 0 to 10 °C with $PM_{2.5}$ mass concentrations mostly at around 50 μg m^{-3}. At the end of the heating season, the temperature gradually increased to 10–30 °C, with $PM_{2.5}$ mass concentrations of around 25 μg m^{-3}. On the one hand, we speculated that this change was mainly attributed to the larger emission of PM due to the cold heating seasons; on the other hand, the gradual increased temperature is favorable for atmospheric turbulence, which causes a decrease in PM near the ground. The distribution of RH with $PM_{2.5}$ has been shown in Fig. 4. During the heating season, the higher RH was nearly 80% with the $PM_{2.5}$ increasing to 250 μg m^{-3}. In the transition and non-heating season s, the lower RH value corresponded to a $PM_{2.5}$ mass concentration of around 50 μg m^{-3}. Tang et al. (2015) indicated that high RH may favor local contribution of humidity-related physicochemical processing during heavy pollution periods.

In Fig. 4 we present scatter plots of SO_2–$PM_{2.5}$, NO_2–$PM_{2.5}$, O_3–$PM_{2.5}$, CO–$PM_{2.5}$, O_3—NO_2 and SO_2—NO_2 based on the whole heating season. There was a strong positive correlation between SO_2 and $PM_{2.5}$ in the heating season, and became weaker in the transition and non-heating season. The SO_2 displayed a strong increase in the heating season from 20 to 100 μg m^{-3}, but there was a significant decrease in the end of the heating range to < 20 μg m^{-3}. This result emphasizes the role of coal consumption for heating as the main contributor of SO_2 pollution, as mentioned in Section 3.1. The changes in slope among $PM_{2.5}$ and SO_2 imply that $PM_{2.5}$ was highly associated with SO_2 in the heating season, then the secondary reactions with particles during the transition and non-heating season, leading to a weakened correlation between $PM_{2.5}$ and SO_2.

A positive correlation was found between $PM_{2.5}$ and NO_2/CO during the three stages in the whole heating season, which suggested that $PM_{2.5}$ was highly correlated with NO_2 and CO from both fossil combustion and biomass burning in northeastern China. A scatter plot of O_3 with $PM_{2.5}$ for the different periods is shown in Fig. 4. During the heating season, a negative correlation was found under low air temperatures. From the transition period to the end of the heating season, a significant positive correlation was observed between O_3 and $PM_{2.5}$, which was associated with the formation of secondary aerosols with higher O_3 concentrations and the photooxidation (Kamens et al., 1999; Lambe et al., 2015; Palm et al., 2017). A negative correlation between O_3 and NO_2 was found in the heating season, whereas a positive

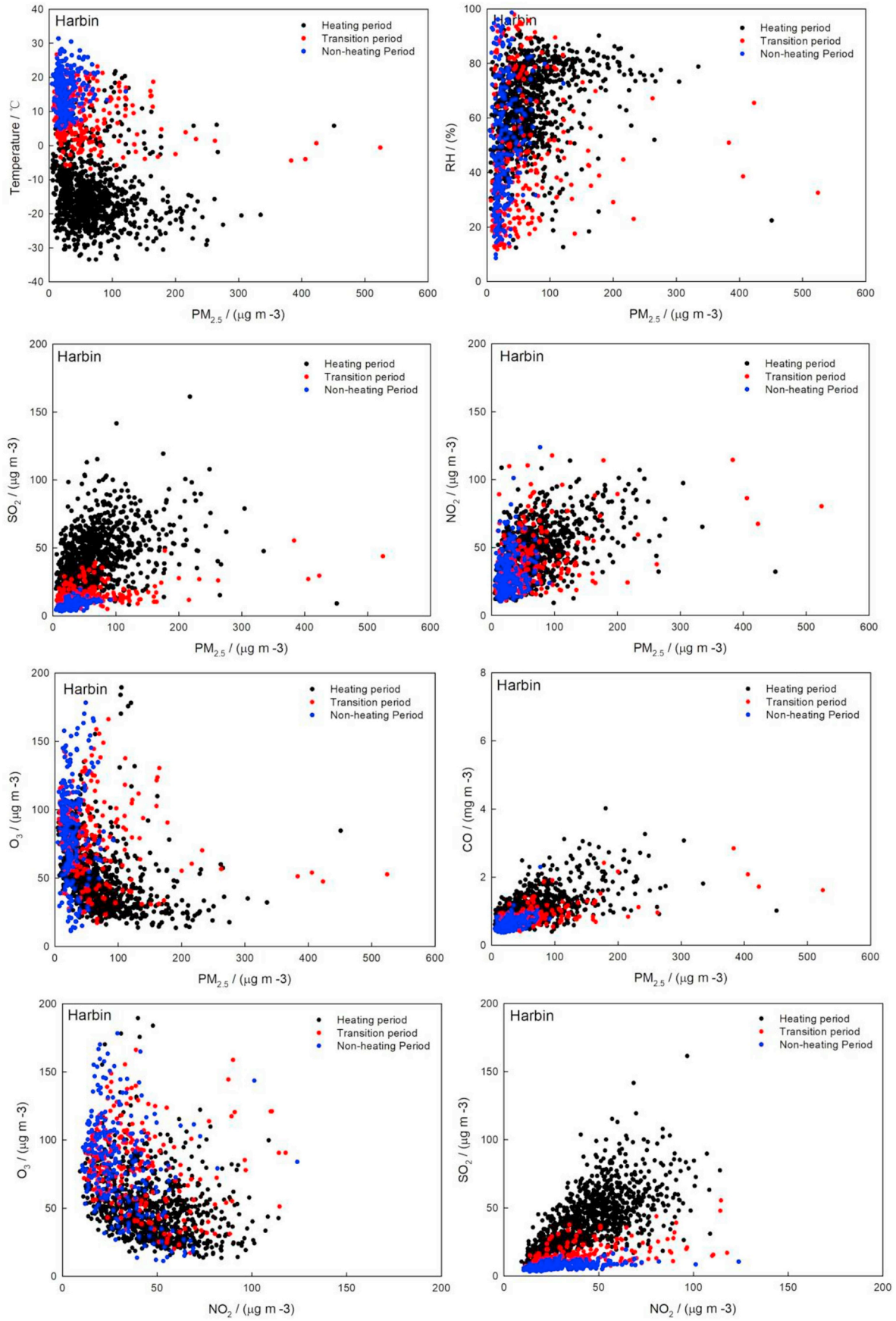

Fig. 4. Relationship between PM and gaseous pollutants during the different heating stages at Harbin, Changchun and Siping. See Fig. 3 for an explanation of the heating stages.

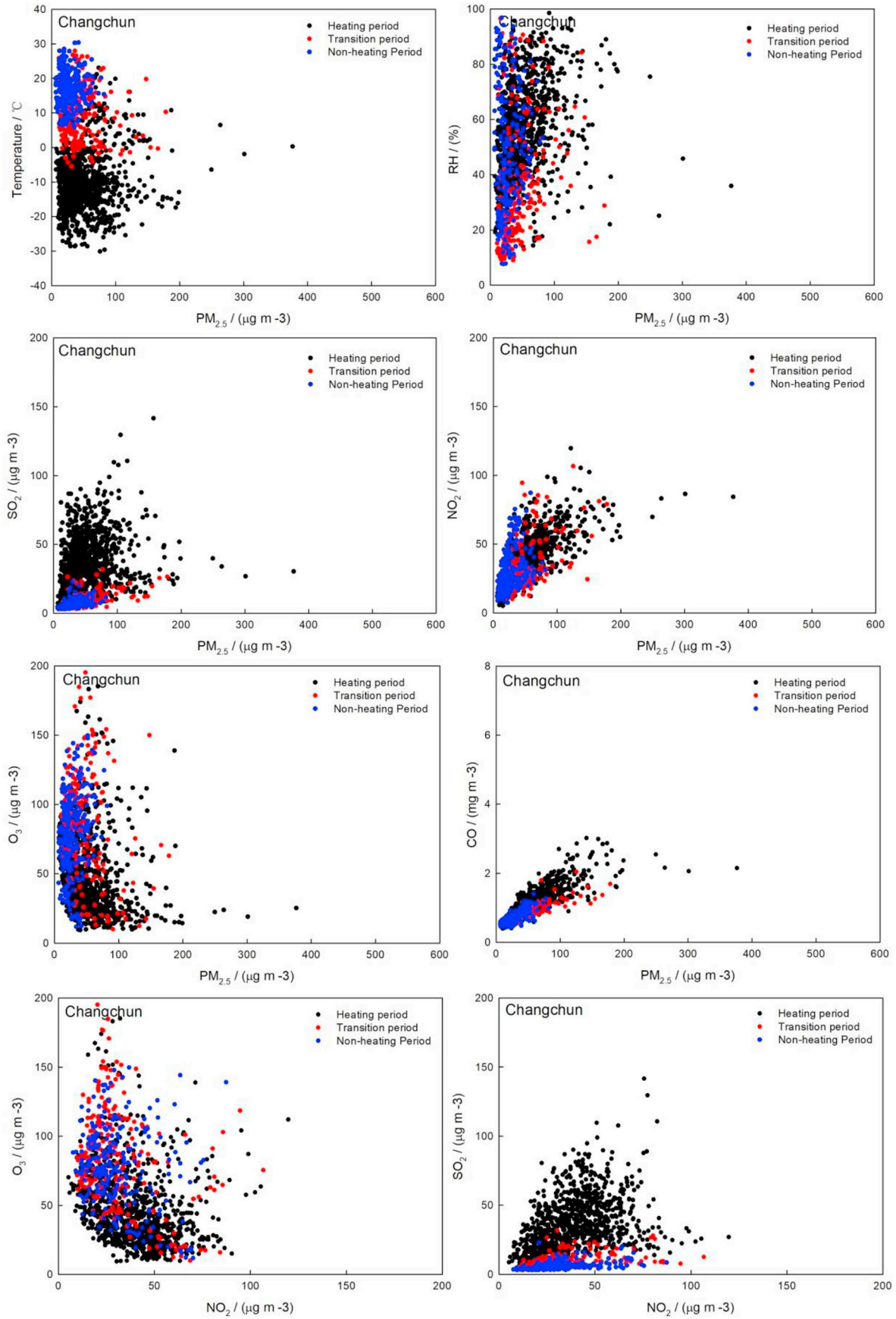

Fig. 4. (*continued*)

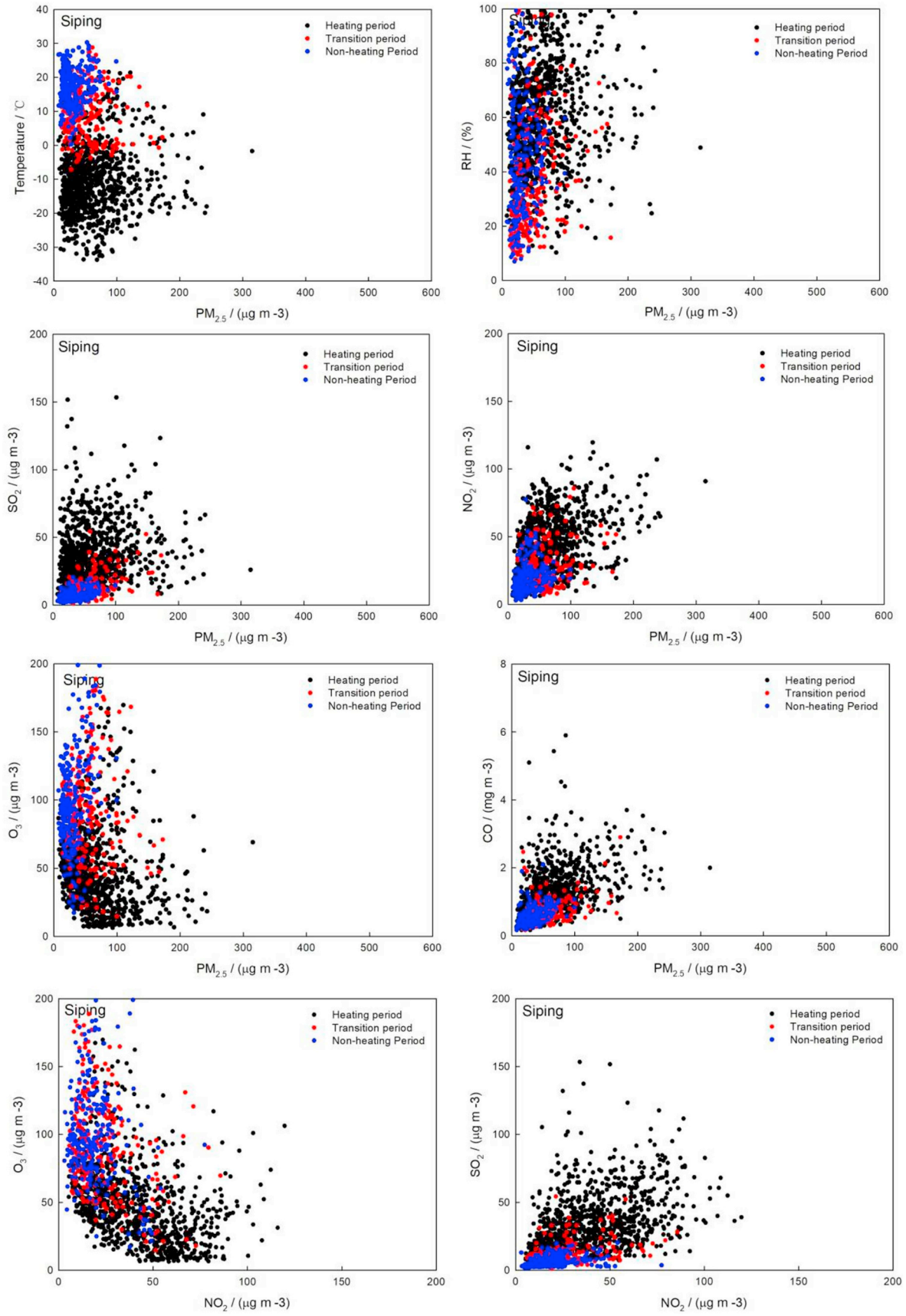

Fig. 4. (*continued*)

correlation was observed at the end of the heating season (Fig. 4). This could be due to the photochemical reactions of O_3 in the presence of sunlight with higher temperatures. There was a significant positive correlation between SO_2 and NO_2 in the heating season. The weaker correlation implied the no significant association with SO_2 and NO_2 in the transition and non-heating seasons. These changes could be due to the different sources of SO_2 and NO_2. The heavy loading of SO_2 was mainly attributed to the coal consumption in the heating season and dropped rapidly in the transition and non-heating season. The NO_2 emissions were associated with petroleum fuel consumption, which was maintained throughout the year.

These findings indicate that coal combustion during heating season could cause some considerable changes to PM and gas pollutant concentrations, which was different from the findings for the transition and non-heating season. In addition to the kinetic conditions, the thermodynamic conditions at different stages have an active effect on accelerating the transformation of primary gaseous pollutants. Temperature could be considered one of the important environmental elements responsible for removal and conversion of gaseous pollutants during different residential heating processes by controlling the degree of photochemical reaction.

3.5. Diurnal variation of PM and gas pollutants during the different heating stages

Fig. 5 shows the diurnal patterns of the air pollutants during the heating seasons in the Harbin-Changchun megalopolis based on local time (LT). The investigation of diurnal pollutants concentrations within a day was conducted to further analyze source contribution.

The diurnal variation of $PM_{2.5}$ was generally higher in the heating and transition periods than in the non-heating season at the three sites. The $PM_{2.5}$ mass concentrations at Harbin showed clear diurnal changes. The average mass concentration of $PM_{2.5}$ was 95.8 $\mu g\,m^{-3}$ at 09:00 LT and then reduced to about 41.5 $\mu g\,m^{-3}$ at 15:00 LT with a twice reduction in the heating season at Harbin. The variation of $PM_{2.5}$ was similar in Changchun and Siping, but there was a time lag on the peak value occurrence in Siping, which occurred at 11:00 LT and 22:00 LT. The later time of $PM_{2.5}$ peak values in Siping may be due to the slower pollutant accumulation because of the reduced anthropogenic activity and consumption of coal in this region during the heating season. In Harbin, the diurnal variations of PM_{10} during the heating and transition periods were consistently higher than those in the non-heating season. The peak value of PM_{10} occurred at 09:00 LT and 20:00 LT. Unlike Harbin, the concentrations of PM10 in Changchun and Siping increased significantly in the transitional period. The PM10 generally increased from 08:00 LT and had a maximum value at 17:00 LT and maintained with an overall range about 80–100 $\mu g\,m^{-3}$. The diurnal variation of moderate increase of PM_{10} concentrations in Changchun and Siping may be generally affected by the coarse mode particles in the transition period. According to Zhao et al. (2015, 2018), this phenomenon could also be attributed to the diurnal patterns of the meteorological conditions.

The diurnal fluctuation trend of NO_2 at different stages showed essentially the same pattern in the three regions: heating season > transition season > non-heating season. The NO_2 in the heating season was about 1.6, 1.3 and 2.2 times higher than that in other two periods in Harbin, Changchun and Siping, respectively. At the three sites, NO_2 showed a clear peak at 07:00 LT to 08:00 LT in the early morning and 19:00 LT in the evening. This indicates that the pollutant emissions in heating season were not the main factor controlling NO_2 diurnal variation in northeastern China. The diurnal pattern of NO_2 concentration could also be due to the local traffic conditions caused by the rush hour and regional biomass burning during the sampling period. SO_2 is one of the main pollutants emitted by coal burning in northeastern China, and it was found to have substantially lower concentrations in the transitional and non-heating season in three regions. The diurnal variation of SO_2 concentrations in the heating season was about 5.8, 5.9 and 5.2 times as high as that in the other two stages in Harbin, Changchun and Siping, respectively. During the heating season, the peak values of SO_2 occurred at 09:00–10:00 LT and 20:00 LT, with the maximum value ranging from 40 to 60 $\mu g\,m^{-3}$ at the three sites. The peak time of SO_2 was about 1–2 h later than that of NO_2, indicating that the two pollutants were associated with different sources. The diurnal CO mass concentration in the three regions decreased in the order heating season > transitional period > non-heating season. The diurnal pattern (peak values at 09:00 LT and 20:00 LT) corresponded to the morning and evening rush hours. The daily variation of CO is likely to be due to incomplete fossil fuel combustion, which mainly originates from ground-level vehicle emissions.

The mass concentration of O_3 showed the opposite diurnal variation to the other pollutants. The O_3 concentrations in the transition and non-heating season s were very similar, and the diurnal changes were significantly higher than those in the heating season. The O_3 mass concentration was 1.6–2.0 times higher in the transition and non-heating seasons than the heating seasons in Harbin, Changchun and Siping. The O_3 mass concentration increased gradually from 10:00 LT to a maximum value at 16:00–17:00 LT and maintained a high value of more than 100 $\mu g\,m^{-3}$. These results show a major influence on diurnal variation of O_3 after the heating activity decreased in the three regions as a result of the longer and stronger solar irradiation in the daytime, contributing to photochemical formation.

3.6. Case studies

The temporal variation in PM and gaseous pollutant concentrations and aerosol vertical profiles detected by ground-based lidar were used to analyze the comprehensive characteristics of air pollution during the heating season in the Harbin-Changchun megalopolis, northeastern China. We focused on the development process of intense aerosol pollution in 24 h during 12:00 LT 31 December to 12:00 LT 1 January for a case analysis (Fig. 6).

In general, we found a pollution development process across Siping, Changchun and Harbin. The maximum hourly $PM_{2.5}$ and PM_{10} concentrations first appeared at 20:00–22:00 LT in 31 December 2017 over Siping, with peak values of 310.0–334.5 and 211.0–253.7 $\mu g\,m^{-3}$, respectively; then the peak value of $PM_{2.5}$ (239.1–239.9 $\mu g\,m^{-3}$) and PM_{10} (172.6–180.3 $\mu g\,m^{-3}$) were recorded at 22:00 LT 31 December 2017–00:00 LT 1 January 2018 in Changchun; in Harbin, the peak value of $PM_{2.5}$ and PM_{10} has been found at 10:00 to 12:00 LT 1 January 2018 about 283.8–320.0 and 225.1–258.1 $\mu g\,m^{-3}$, respectively. The hourly mass concentration of CO, NO_2 and SO_2 has the same trend as particulate matter in this case. The 1000-hPa wind fields on 1 January 2018 at 08:00 LT were more conducive to the pollutant aerosols transportation southwesterly from Siping to Harbin, passing Changchun (Fig. 11). This possible pollution transition process in Northeastern China has also been reported by Li et al. (2015).

We used the 72-h back trajectory clustering along with the WPSCF/WCWT analysis to further investigate the contribution of local emission and regional transportation during this period over the Harbin-Changchun megalopolis. As shown in Fig. 7a, we found the main clusters came from the local area and northwest regions during the pollution period.

During the pollution period, trajectories with short transport and slow-moving patterns were found in Harbin, Changchun, and Siping, contributing to the proportion about 27.08%, 48.96% and 22.92% of the total pollution from location and nearby, respectively. The typical clusters in the heating season indicate the air pollutant sources from Heilongjiang, Jilin and Liaoning provinces, which then accumulated in

the Harbin-Changchun megalopolis. The long and fast-moving trajectories originated from Northwest China, contributing to 51.04% (37.50% + 13.54%) and 77.09% (28.13% + 48.96%) of the total pollution in Changchun and Siping. This result indicates a unique climatic feature in northeast China, which was significantly affected by the airflow from the northwest region in winter and spring (Zhang et al., 2018b). Larger spatial potential $PM_{2.5}$ sources were shown in Harbin, Changchun and Siping during the heating season (Fig. 7b), with high WPSCF values of > 0.9 from the surrounding area. This pattern indicated some local pollutant contributions in these three cities. The WCWT analysis also showed the relatively higher pollutant concentration in the local cites at the same time (Fig. 7c). Therefore, the changes in the air pollutant trajectories and the area of WPSCF/WCWT values could reflect the contribution of the main potential source of $PM_{2.5}$

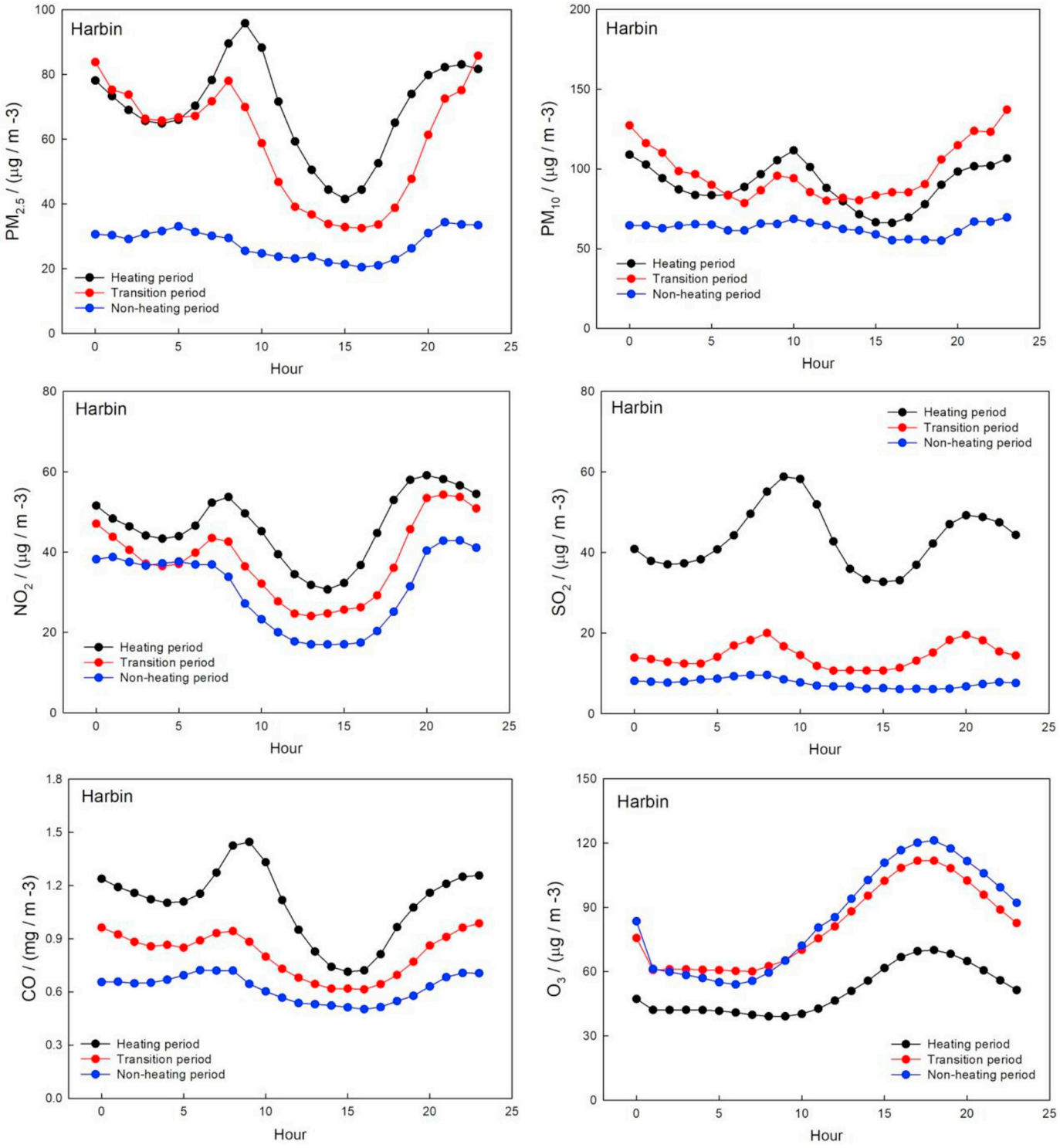

Fig. 5. Diurnal variation of PM and gaseous pollutants during the different heating stages at Harbin, Changchun and Siping.

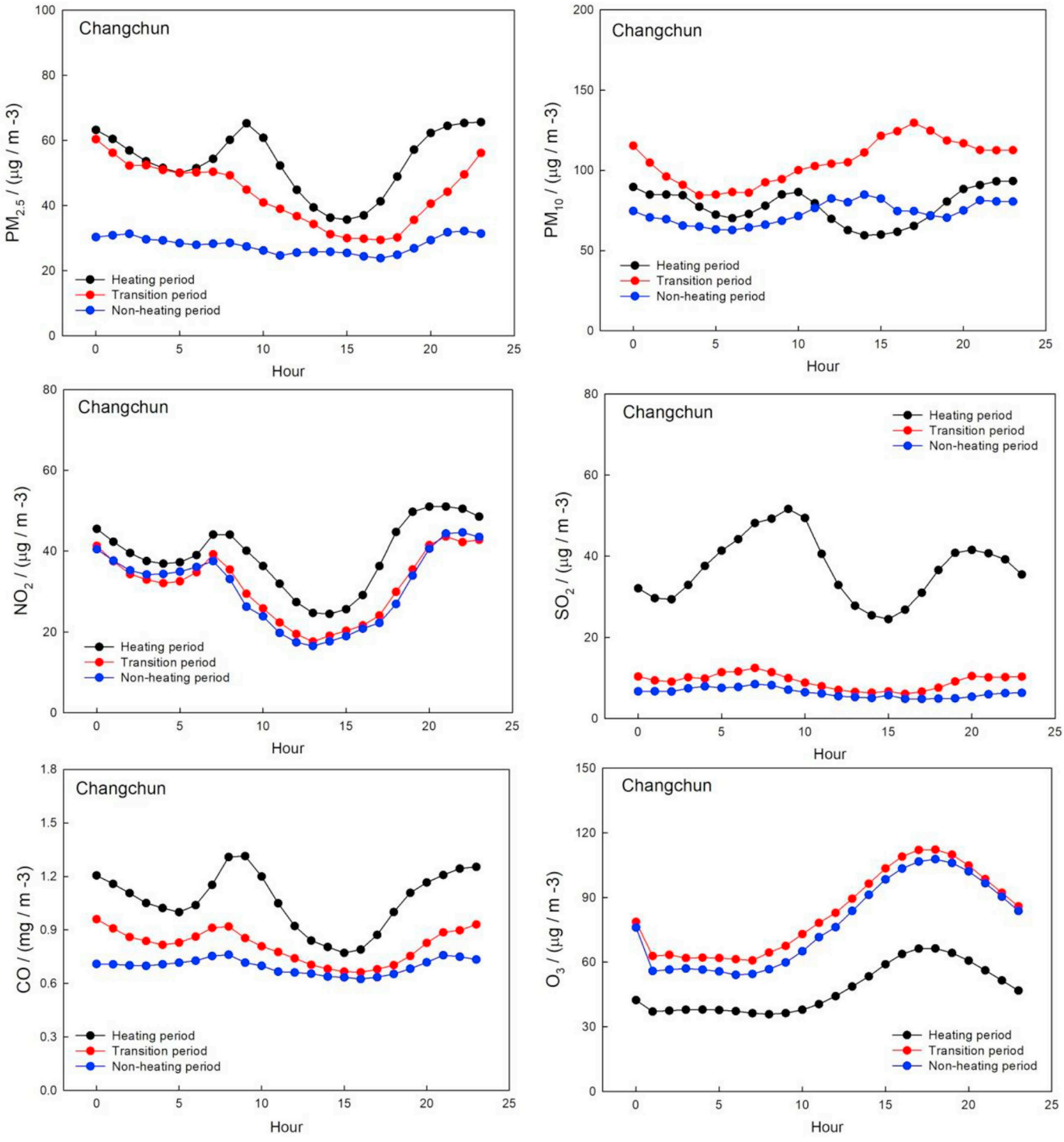

Fig. 5. (*continued*)

from the local and regional emissions in and around the Harbin-Changchun megalopolis during the pollution period.

Figs. 8and9 shows the time–height cross-section of the ground-based lidar and the aerosol extinction coefficient evolution process from the vertical structure of the lidar measurements. We calculated the extinction coefficient below 2 km to quantitatively assess the contribution of aerosols to the pollution.

During the pollution episode, we found that there were two layers of extinction coefficients, occurring near the ground and at a height of approximately 800–1000 m. The extinction coefficient was found to be higher than about 0.9 km^{-1} near the surface (200 m) and 0.5 km^{-1} at 1080 m at 12:00 LT on 31 December 2017 over Harbin. As time progressed, the aerosol layer with the extinction coefficient decreased to about 0.3 km^{-1} at 500 m from 16:00 to 20:00 LT. Then at the beginning of 1 January 2018 from 00:00 LT to 04:00 LT, the extinction coefficient in the upper layer gradually increased from 0.2 km^{-1} at 600 m to about 0.3 km^{-1} at 700 m. During this time, the near-surface pollution was reduced, with a smaller extinction coefficient of about 0.5–0.7 km^{-1}. At

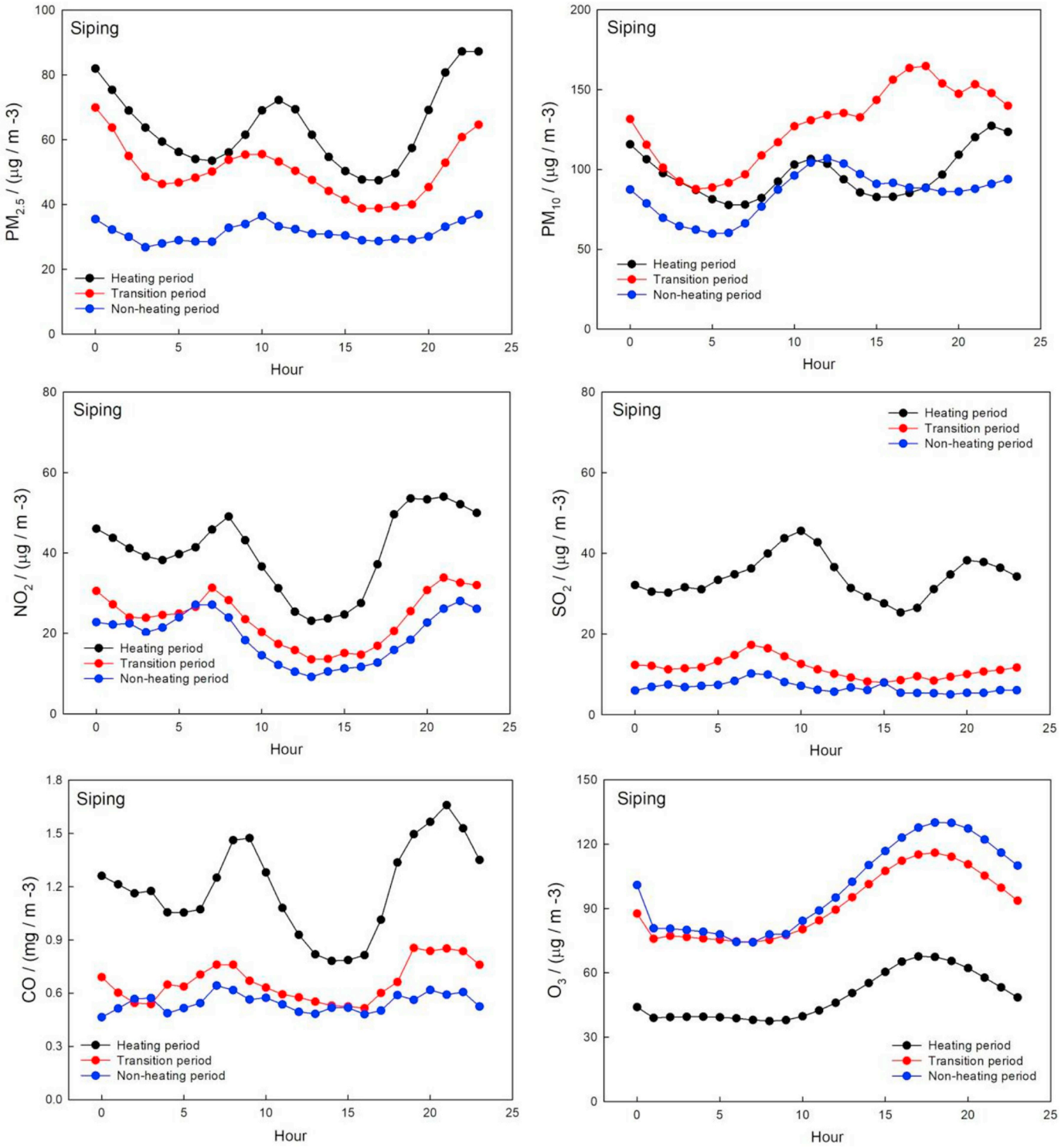

Fig. 5. (*continued*)

12:00 LT on 1 January 2018, the pollution near the ground intensified again with an extinction coefficient of about 1.0 km^{-1} at 200 m. The PBL was mostly below 200 m at 11:00 LT on 1 January 2018 (Fig. 10a). The shallow PBL heights for this episode could lead to high aerosol concentration in the near-surface layer.

Unlike the variation of the two extinction layers in upper and surface at Harbin, a combination of the two extinction layers in the upper was found in Yushu. Combined with the PBL data, these findings indicated a distinct aerosol extinction layer descending towards the ground in this region. At the beginning, there were two aerosol extinction layers, about 0.1 km^{-1} at 800 m and 0.4 km^{-1} near the surface, that occurred on 31 December 2017 at 12:00 LT over Yushu. The extinction layer then gradually reduced to a height of approximately 500 m, with larger extinction coefficient of about 0.2 km^{-1} at 20:00 LT on 31 December 2017. Then the PBL height decreased rapidly from 1400 to > 500 m at 23:00 LT on 31 December 2017 (Fig. 10b). After

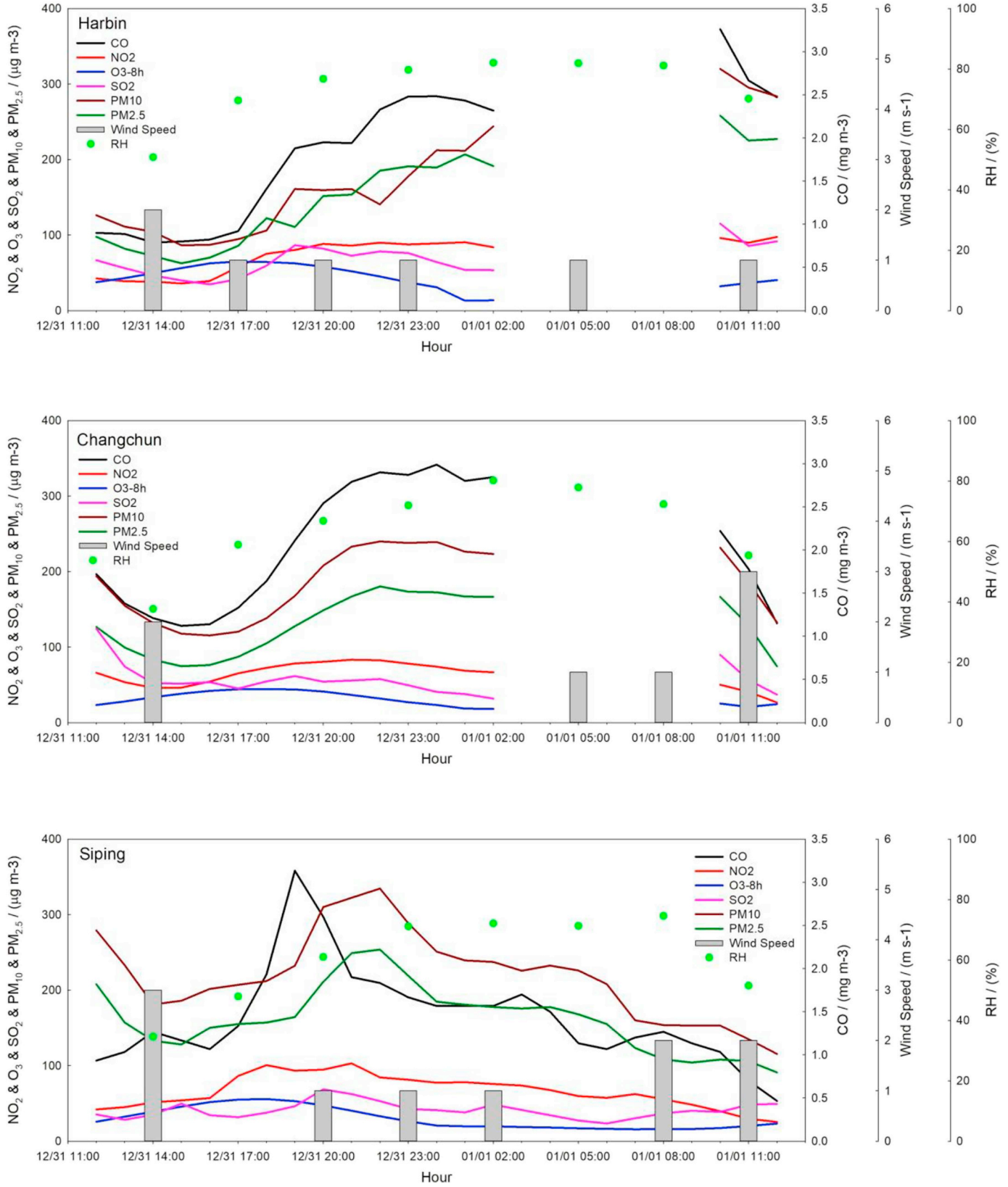

Fig. 6. Hourly air pollutants and meteorological elements during the pollution event (31 December 2017 to 1 January 2018) at Harbin, Changchun and Siping.

00:00 LT on 1 January 2018, the aerosol extinction layer decreased to the ground, with the larger extinction coefficient of 0.4 km^{-1} appearing at 08:00 LT. This pattern of extinction coefficient indicates the combination of two aerosol extinction layers in this event.

The case study showed that the local emissions in the ground and the aerosol convective activities both contributed to the aerosol extinction and air pollution in the Harbin-Changchun megalopolis.

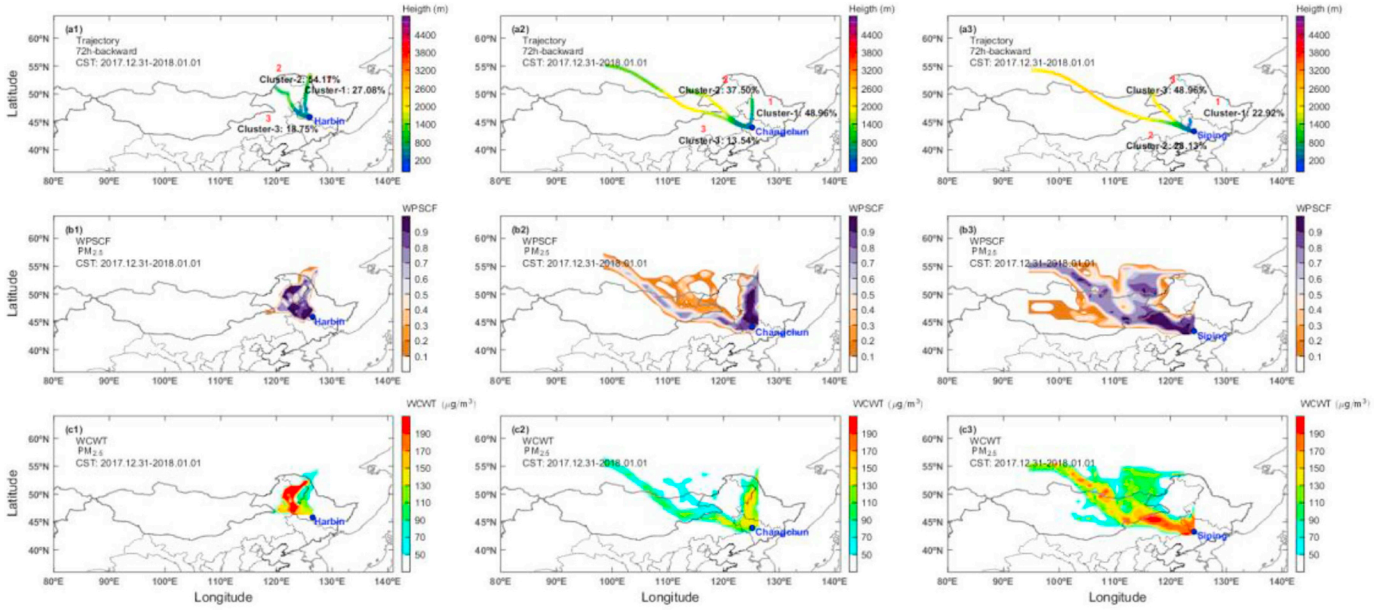

Fig. 7. The (a) 72-h backward trajectories and spatial distributions of (b) WPSCF and (c) WCWT values for $PM_{2.5}$ in the pollution event (31 December 2017 to 1 January 2018) at Harbin, Changchun and Siping.

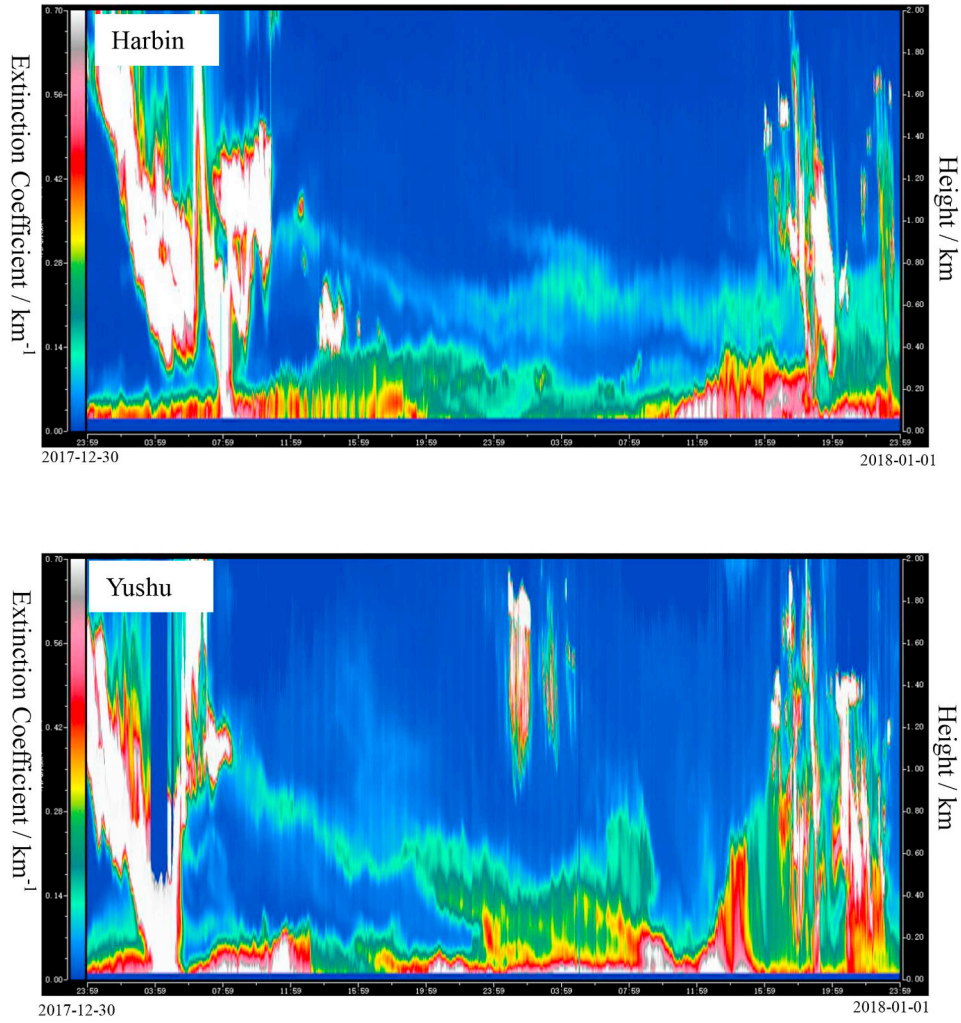

Fig. 8. Time–height cross section of aerosol extinction coefficients during the pollution event (31 December 2017 to 1 January 2018) at Harbin and Yushu.

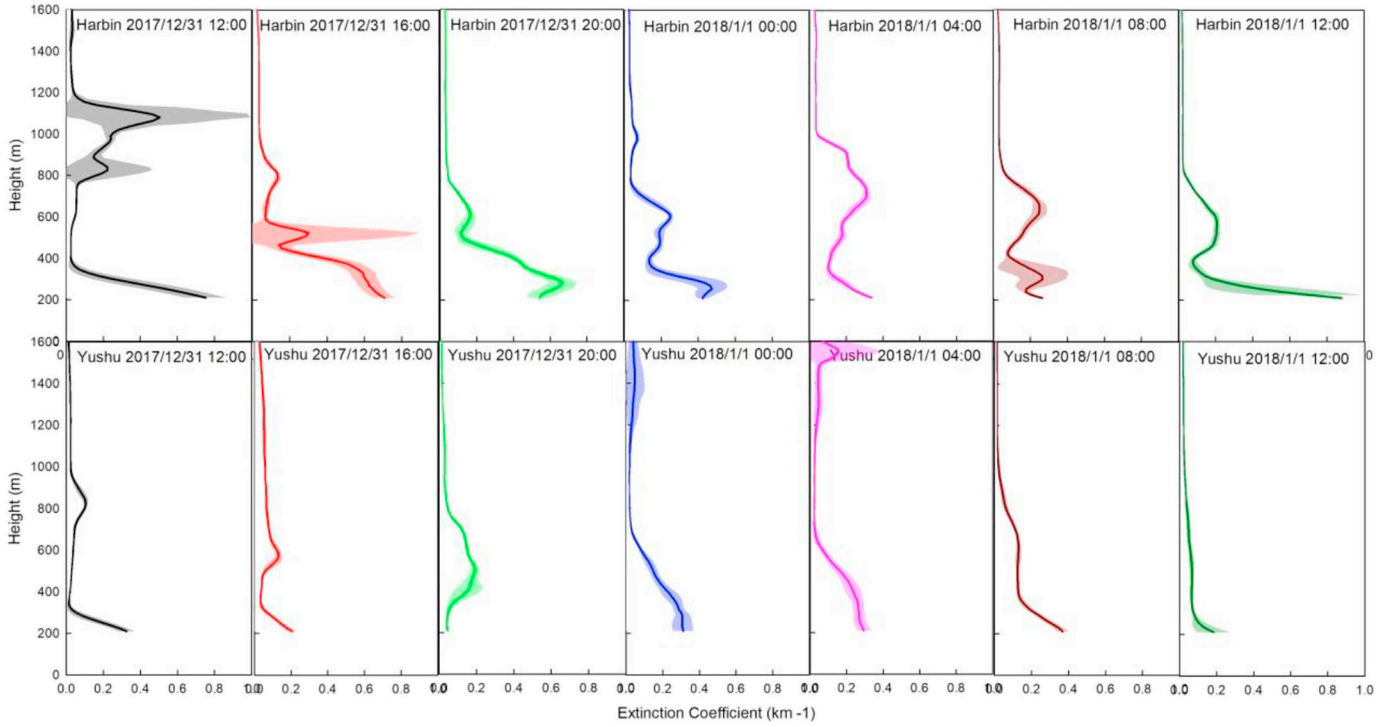

Fig. 9. Vertical profiles of the extinction coefficient during the pollution event (31 December 2017 to 1 January 2018) at Harbin and Yushu. The shaded area represents the standard deviations of the arithmetic means.

4. Conclusions

Temporal variation of PM and gas pollutants, as well as the relationship with meteorological elements during the whole heating season was determined for 1 December 2017 to 31 May 2018 at three sites in the Harbin-Changchun megalopolis, northeastern China. The air backward trajectory and aerosol vertical profiles detected with ground-based lidar were also provided to assess the pollutant potential sources during the whole heating season. The first conclusion of this study indicated that pollutant days were concentrated in the heating season with higher concentration of fine-mode particles and sharply increased SO_2 which could act as an indicator of the air quality in the Harbin-Changchun megalopolis during heating activities.

Secondly, the strong wind in the sampling period could help to lead regional transportation and causing air quality deterioration and the apparent temperature changes according to the solar radiation might be the main factor effects on secondary formation of aerosol and the chemical transformation of gaseous pollutants.

The thermodynamic conditions at different coal combustion stages could be considered one of the important environmental elements responsible for removal and conversion of gaseous pollutants during different residential heating processes. The diurnal variation of pollutant could require more consideration on the local traffic conditions and the rush hour.

Larger spatial potential $PM_{2.5}$ sources indicated significant local pollutant contributions to the heating season regionally. The aerosol extinction coefficient and corresponding PBL evolution process from the vertical structure of the lidar measurements revealed a combination of the local emissions in the ground-surface and the aerosol convective activities resulted in aerosol extinction and air pollution by the mixture

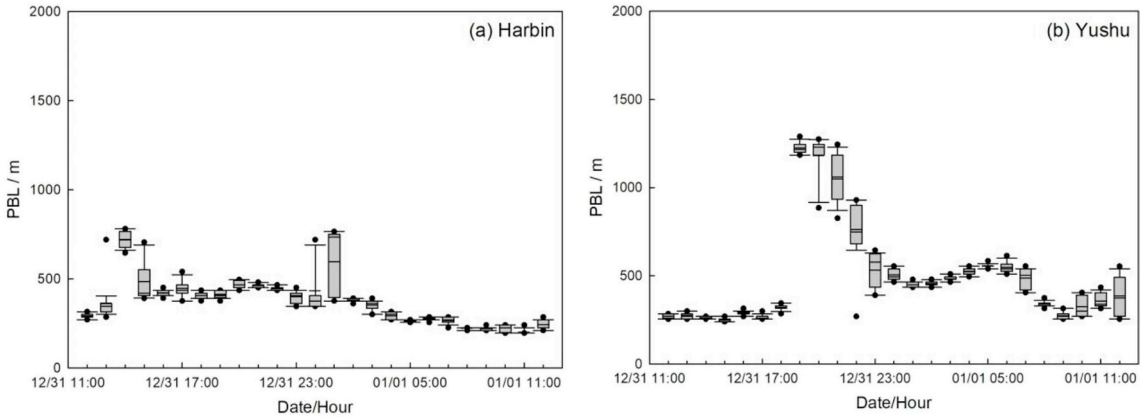

Fig. 10. Temporal and spatial distribution of the PBL height during the pollution event (31 December 2017 to 1 January 2018) at Harbin and Yushu. The whiskers show the 5th and 95th percentiles, and the black dots indicate the 1st and 99th percentiles. The dots and solid lines within the box represent the mean and median values, respectively.

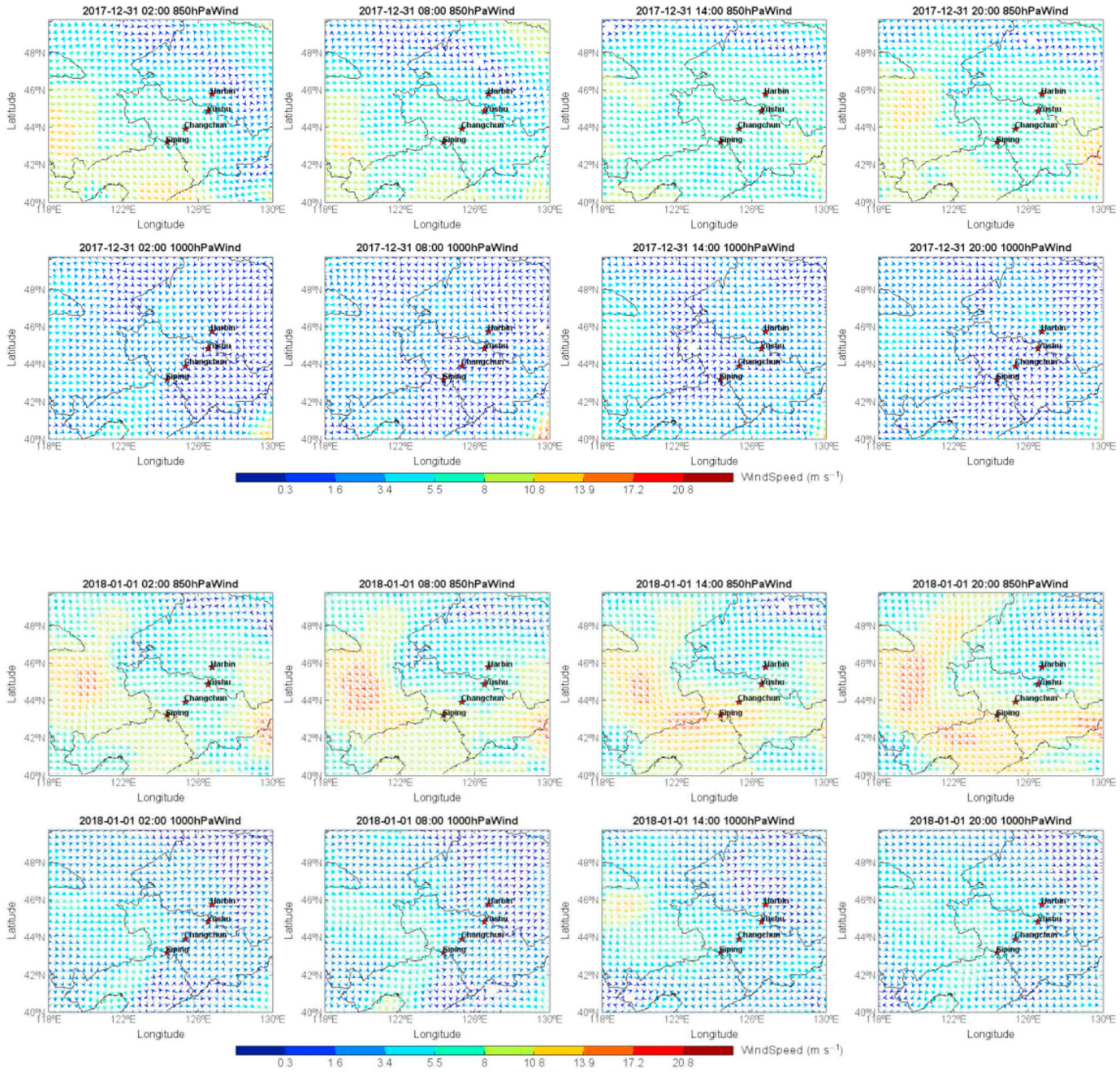

Fig. 11. Variation of the wind field at 850 and 1000 hPa during the pollution event (31 December 2017 to 1 January 2018) in the Harbin-Changchun megalopolis, northeastern China.

effect in the Harbin-Changchun megalopolis, northeastern China.

The findings of this study could provide useful information on the characteristics of PM and gaseous pollutants as well as indicating the potential pollutant source from anthropogenic activities during the heating season in northeastern China. These findings may be helpful for pollutant emission control and air quality improvement and the collected data can act as an important dataset for model simulations in future research.

Acknowledgments

This work is financially supported by grant from National Key Research and Development Program of China 2017YFC0212301, National Natural Science Foundation of China (41605112, 41825011 & 41875157), National Key R&D Program of China (2016YFA0601901), National Natural Science Foundation of China (41590874), and the CAMS Basis Research Project (2017Z011).

Appendix A. Supplementary data

Supplementary data to this article can be found online at https://doi.org/10.1016/j.jastp.2019.03.001.

References

Andreae, M.O., Gelencsér, A., 2006. Black carbon or brown carbon? The nature of light-absorbing carbonaceous aerosols. Atmos. Chem. Phys. 6, 3131–3148. https://doi.org/10.5194/acp-6-3131-2006.

Bahadur, R., Habib, G., Russell, L.M., 2009. Climatology of PM2.5 organic carbon concentrations from a review of ground-based atmospheric measurements by evolved gas analysis. Atmos. Environ. 43, 1591–1602.

Bond, T.C., Streets, D.G., Yarber, K.F., Nelson, S.M., Woo, J.H., Klimont, Z., 2004. A technology-based global inventory of black and organic carbon emissions from combustion. J. Geophys. Res. 109, D14203. https://doi.org/10.1029/2003JD003697.

Cao, G.L., Zhang, X.Y., Zheng, F.C., 2006. Inventory of black carbon and organic carbon emissions from China. Atmos. Environ. 40, 6516–6527. https://doi.org/10.1016/j.atmosenv.2006.05.070.

Chen, S.R., Xu, L., Zhang, Y.X., Chen, B., Wang, X.F., Zhang, X.Y., Zheng, M., Chen, J.M., Wang, W.X., Sun, Y.L., Fu, P.Q., Wang, Z.F., Li, W.J., 2017. Direct observations of organic aerosols in common wintertime hazes in North China: insights into direct emissions from Chinese residential stoves. Atmos. Chem. Phys. 17, 1259–1270. https://doi.org/10.5194/acp-17-1259-2017.

Chen, Q., Yuan, Y., Huang, X., He, Z., Tan, H., 2018. Assessment of column aerosol optical properties using ground-based sun-photometer at urban Harbin. Northeast China. J. Environ. Sci. 74, 50–57.

Hennigan, C.J., Bergin, M.H., Dibb, J.E., Weber, R.J., 2008. Enhanced secondary organic aerosol formation due to water uptake by fine particles. Geophys. Res. Lett. 35, 102.

Huang, L., Wang, G., 2014. Chemical characteristics and source apportionment of atmospheric particles during heating period in Harbin, China. J. Environ. Sci. 26, 2475–2483.

Kamens, R., Jang, M., Chien, C.J., Leach, K., 1999. Aerosol formation from reaction of α-pinene and ozone using a gas-phase kinetics-aerosol partitioning model. Environ. Sci. Technol. 33, 1430–1438.

Kirpa, R., Sarin, M.M., 2011. Day-night variability of EC, OC, WSOC and inorganic ions in urban environment of Indo-Gangetic Plain: implications to secondary aerosol formation. Atmos. Environ. 45, 460–468.

Kong, S.F., Ji, Y.Q., Lu, B., Bai, Z.P., Chen, L., Han, B., Li, Z., 2012. Chemical compositions and sources of atmospheric PM10 in heating, non-heating and sand periods at a coal-based city in northeastern China. J. Environ. Monit. 14, 852–865.

Lambe, A.T., Chhabra, P.S., Onasch, T.B., Brune, W.H., Hunter, J.F., Kroll, J.H., Cummings, M.J., Brogan, J.F., Parmar, Y., Worsnop, D.R., Kolb, C.E., Davidovits, P., 2015. Effect of oxidant concentration, exposure time, and seed particles on secondary organic aerosol chemical composition and yield. Atmos. Chem. Phys. 15, 3063–3075. https://doi.org/10.5194/acp- 15-3063-2015.

Li, Y., Zhao, H., Wu, Y., 2015. Characteristics of particulate matter during haze and fog (pollution) episodes over Northeast China, Autumn 2013. Aerosol. Air. Qual. Res. 15, 853–864. https://doi.org/10.4209/aaqr.2014.08.0158.

Li, Q., Jiang, J.K., Wang, S.X., Rumchev, K., Mead-Hunter, R., Morawska, L., Hao, J.M., 2017a. Impacts of household coal and biomass combustion on indoor and ambient air quality in China: current status and implication. Sci. Total Environ. 576, 347–361. https://doi.org/10.1016/j.scitotenv.2016.10.080.

Li, K.W., Chen, L.H., Ying, F., White, S.J., Jang, C., Wu, X.C., Gao, X., Hong, S.M., Shen, J.D., Azzi, M., Cen, K.F., 2017b. Meteorological and chemical impacts on ozone formation: a case study in Hangzhou, China. Atmos. Res. 196, 40–52. https://doi.org/10.1016/j.atmosres.2017.06.003, 2017.

Li, X., Wu, J., Elser, M., Feng, T., Cao, J., El-Haddad, I., Huang, R., Tie, X., Prévôt, A.S.H., Li, G., 2018. Contributions of residential coal combustion to the air quality in BeijingTianjin-Hebei (BTH), China: a case study. Atmos. Chem. Phys. 18, 10,675–10,691. https://doi.org/10.5194/acp-18-10675-2018.

Li, L., Wu, Y., Xiao, H., Zhang, R., Lin, H., Zhang, X., Kao, S.-J., 2019. Origins of aerosol nitrate in Beijing during late winter through spring. Sci. Total Environ. 653, 776–782.

Liu, J., Mauzerall, D.L., Chen, Q., Zhang, Q., Song, Y., Peng, W., Klimont, Z., Qiu, X., Zhang, S., Hu, M., Lin, W., Smith, K.R., Zhu, T., 2016. Air pollutant emissions from Chinese households: a major and underappreciated ambient pollution source. Proc. Natl. Acad. Sci. Unit. States Am. 113, 7756–7761. https://doi.org/10.1073/pnas.1604537113.

Megido, L., Suárez-Peña, B., Negral, L., Castrillón, L., Fernández-Nava, Y., 2017. Suburban air quality: human health hazard assessment of potentially toxic elements in PM10. Chemosphere 177, 284–291.

NBSC, 2016. National Bureau of Statistics of China. China Statistical Yearbook-2016. China Statistics Press, Beijing.

Ningombam, Shantikumar S., Bagare, S.P., Srivastava, A.K., Sohn, B.J., Song, H.-J., Larson, E., 2014. Aerosol radiative forcing over a high-altitude station Merak, in the trans-Himalayan region during advection of anthropogenic events from the Indo-Gangetic Plain. Atmos. Environ. 98, 253–259.

Ningombam, Shantikumar S., Bagare, S.P., Khatri, P., Sohn, B.J., Song, H.-J., 2015. Estimation of aerosol radiative forcing over an aged-background aerosol feature during advection and non-advection events using a ground-based data obtained from a Prede Skyradiometer observation. Atmos. Res. 164–165, 76–83.

Okada, K., Ikegami, M., Zaizen, Y., Makino, Y., Jensen, J.B., Gras, J.L., 2001. The mixture state of individual aerosol particles in the 1997 Indonesian haze episode. J. Aerosol Sci. 32, 1269–1279.

Palm, B.B., Campuzano-Jost, P., Day, D.A., Ortega, A.M., Fry, J.L., Brown, S.S., Zarzana, K.J., Dube, W., Wagner, N.L., Draper, D.C., Kaser, L., Jud, W., Karl, T., Hansel, A., GutiérrezMontes, C., Jimenez, J.L., 2017. Secondary organic aerosol formation from in situ OH, O3, and NO3 oxidation of ambient forest air in an oxidation flow reactor. Atmos. Chem. Phys. 17, 5331–5354. https://doi.org/10.5194/acp-17-5331-2017.

Pathak, R.K., Wu, W.S., Wang, T., 2009. Summertime PM2.5 ionic species in four major cities of China: nitrate formation in an ammonia-deficient atmosphere. Atmos. Chem. Phys. 9, 1711–1722.

Qiao, J.J., Qi, J.H., Liu, M.M., Fan, D.G., Shi, J.H., Gao, H.W., 2010. Distribution of atmospheric particulate inorganic nitrogen in different weather conditions in the heating period in Qingdao. Environ. Sci. 31, 29–35.

Shen, Z.X., Wang, X., Zhang, R.J., Ho, K.F., Cao, J.J., Zhang, M.G., 2011. Chemical composition of water–soluble ions and carbonate estimation in spring aerosol at a semi–arid site of Tongyu, China. Aerosol. Air. Qual. Res. 11, 360–368.

Shen, G., Wei, S., Zhang, Y., Wang, B., Wang, R., Shen, H., Li, W., Huang, Y., Chen, Y., Chen, H., Tao, S., 2013. Emission and size distribution of particle-bound polycyclic aromatic hydrocarbons from residential wood combustion in rural China. Biomass Bioenergy 55, 141–147. https://doi.org/10.1016/j.biombioe.2013.01.031.

Tang, G., Zhu, X., Hu, B., Xin, J., Wang, L., Münkel, C., Mao, G., Wang, Y., 2015. Impact of emission controls on air quality in Beijing during APEC 2014: lidar ceilometer observations. Atmos. Chem. Phys. 15, 12667–12680.

Tiwari, S., Srivastava, A.K., Bisht, D.S., Bano, T., Singh, S., Behura, S., Srivastava, M.K., Chate, D.M., Padmanabhamurty, B., 2009. Black carbon and chemical characteristics of PM10 and PM2.5 at an urban site of North India. J. Atmos. Chem. 62, 193–209.

Tzompa, S.Z.A., Sullivan, A., Kreidenweis, S.M., 2016. Contribution of biomass burning to carbonaceous aerosols in Mexico City during May 2013. Aerosol. Air. Qual. Res. 16, 114–124.

Wang, G., Wang, H., Yu, Y., Gao, S., Feng, J., Gao, S., Wang, L., 2003. Chemical characterization of water-soluble components of PM10 and PM2:5 atmospheric aerosols in five locations of Nanjing, China. Atmos. Environ. 37, 2893–2902.

Wang, Y.Q., Zhang, X.Y., Arimoto, R., 2006. The contribution from distant dust sources to the atmospheric particulate matter loadings at XiAn, China during spring. Sci. Total Environ. 368, 875–883.

Wang, Y.Q., Zhang, X.Y., Draxler, R.R., 2009. TrajStat: GIS-based software that uses various trajectory statistical analysis methods to identify potential sources from long-term air pollution measurement data. Environ. Model. Softw 24, 938–939.

Watson, J.G., 2002. Visibility: science and regulation. J. Air Waste Manag. Assoc. 52, 628–713.

Zhang, Y.X., Schauer, J.J., Zhang, Y.H., Zeng, L.M., Wei, Y.J., Liu, Y., Shao, M., 2008. Characteristics of particulate carbon emissions from real-world Chinese coal combustion. Environ. Sci. Technol. 42, 5068–5073. https://doi.org/10.1021/es7022576.

Zhang, Q., Streets, D.G., Carmichael, G.R., He, K.B., Huo, H., Kannari, A., Klimont, Z., Park, I.S., Reddy, S., Fu, J.S., Chen, D., Duan, L., Lei, Y., Wang, L.T., Yao, Z.L., 2009. Asian emissions in 2006 for the NASA INTEX-B mission. Atmos. Chem. Phys. 9, 5131–5153. https://doi.org/10.5194/acp-9-5131-2009.

Zhang, R.J., Tao, J., Ho, K.F., Shen, Z.X., Wang, G.H., Cao, J.J., Liu, S.X., Zhang, L.M., Lee, S.C., 2012. Characterization of atmospheric organic and elemental carbon of PM2.5 in a typical semi–arid area of Northeastern China. Aerosol. Air. Qual. Res. 12, 792–802.

Zhang, J., Liu, L., Wang, Y., Ren, Y., Wang, X., Shi, Z., Zhang, D., Che, H., Zhao, H., Liu, Y., Niu, H., Chen, J.-M., Zhang, X., Lingaswamy, A.P., Wang, Z., Li, W., 2017a. Chemical composition, source, and process of urban aerosols during winter haze formation in Northeast China. Environ. Pollut. 231 (Pt 1), 357–366. https://doi.org/10.1016/j.envpol.2017.07.102.

Zhang, Z.Z., Wang, W.X., Cheng, M.M., Liu, S.J., Xu, J., He, Y.J., Meng, F., 2017b. The contribution of residential coal combustion to PM2.5 pollution over China's Beijing-Tianjin-Hebei region in winter. Atmos. Environ. 159, 147–161. https://doi.org/10.1016/j. atmosenv.2017.03.054.

Zhang, G., Xu, H., Qi, B., Du, R., Gui, K., Wang, H., Jiang, W., Liang, L., Xu, L., 2018a. Characterization of atmospheric trace gases and particulate matter in Hangzhou, China. Atmos. Chem. Phys. 18, 1705–1728.

Zhang, Y., Yuan, Q., Huang, D., Kong, S., Zhang, J., Wang, X., Lu, C., Shi, Z., Zhang, X., Sun, Y., Wang, Z., Shao, L., Zhu, J., Li, W., 2018b. Direct observations of fine primary particles from residential coal burning: insights into their morphology, composition, and hygroscopicity. J. Geophys. Res. Atmos. 123. https://doi.org/10.1029/2018JD028988.

Zhao, H., Che, H., Ma, Y., Xia, X., Wang, Y., Wang, P., Wu, X., 2015. Temporal variability of the visibility, particulate matter mass concentration and aerosol optical properties over an urban site in Northeast China. Atmos. Res. 166, 204–212. https://doi.org/10.1016/j.atmosres.2015.07.003.

Zhao, H., Che, H., Xia, X., Wang, Y., Wang, H., Wang, P., Ma, Y., Yang, H., Liu, Y., Wang, Y., Gui, K., Sun, T., Zheng, Y., Zhang, X., 2018. Multi-year ground-based measurements of aerosol optical properties and direct radiative effect over different surface types in northeastern China. J. Geophys. Res. Atmos. 123, 13887–13916. https://doi.org/10.1029/2018JD029141.